Mobile salts reroute sedimentary pathways in the Moroccan Atlantic margin

Remi Charton,

Department of Geoscience and Engineering, Delft University of Technology,

P.O. Box 5048, 2600 GA Delft, The Netherlands

and North Africa Research Group, University of Manchester, UK.

Christian Kluge,

Helmholtz Centre Potsdam - GFZ German Research Centre for Geosciences, Telegrafenberg, 14473 Potsdam, Germany

David Fernández-Blanco,

Consejo Superior de Investigaciones Científicas (CSIC), Instituto de Ciencias del Mar (ICM), Passeig Marítim de la Barceloneta, 37-49, E-08003 Barcelona, Spain.

Aude Duval-Arnould,

School of Earth and Environmental Sciences, The University of Manchester, M13 9PL Manchester, United Kingdom

and North Africa Research Group, University of Manchester, UK.

Giovanni Bertotti,

Department of Geoscience and Engineering, Delft University of Technology,

P.O. Box 5048, 2600 GA Delft, The Netherlands

and North Africa Research Group, University of Manchester, UK.

Abstract

We present a workflow to track topographic grow and sedimentary pathways, and apply it to an halokinetic domain in NW Morocco, around the Essaouira-Agadir Basin. The sedimentary architecture of this basin is strongly influenced by development of Atlasic and Atlantic early Mesozoic riftings. The basin is now part of the Western High Atlas after Alpine exhumation and exposes several salt-cored anticlines perpendicular to the NW Africa coast. We study two of these salt-cored anticlines to understand how their tectonic evolution influence seaward sediment pathways during Mesozoic exhumation of long-lived sedimentary sources in the hinterlands. We gather structural data in Google Earth and use it in Move 2D to derive the thickness of sedimentary units in both E-W salt-cored anticlines. Results show salt mobilisation and topographic growth of these anticlines diverge the sedimentary routing of paleodrainages during the Early to Middle Jurassic exhumation of the Moroccan hinterland, and thus suggest a causal relationship.

Introduction

Salt mobility leading to surface topography influences sediment pathways. Extensive fieldwork and high-resolution 3D seismic surveys document this relationship between halokinesis and sediment channelling in fluvial and shallow-marine environments (e.g., Venus et al., 2015; Rojo and Escalona, 2018), but this relationship is unexplored in onshore areas with scarce field data.

Salt mobility markedly affected the post-rift evolution of the Moroccan passive margin, in NW Africa. A key example is the influence of Triassic salts of the Eastern Diapiric Province in the post-rift sedimentary architecture of Agadir-Essaouira Basin in the western High Atlas (EAB, Fig. 1) (e.g., Michard et al., 2008; Tari et al., 2012). The intense influence of halokinesis in this basin is expressed as salt-cored anticlines in the onshore, allochthonous salt bodies, diapirs and tongues offshore Essaouira, and up-right tear-drop diapirs offshore Agadir (e.g., Hafid et al., 2008; Pichel, 2018). Evidences along two segments of the Central High Atlas suggest that the former basin was intensely deformed by diapirs during the Mesozoic (e.g., Saura et al., 2014; Verges et al., 2017; Moragas et al., 2018).

The EAB evolution is dominated by rifting events, regional exhumation and burial patterns (e.g. Frizon de Lamotte et al., 2009; Domenech, 2015; Ghorbal, 2009; Saddiqi et al., 2009). The former basin developed at the junction between the Central Atlantic and Atlasic riftings during the Triassic to Early Jurassic, and was exhumed during Alpine shortening (e.g., Michard et al., 2008). Presently part of the Western High Atlas, the basin exposes tens of km-long salt-cored anticlines roughly orthogonal to the coast (e.g. Michard et al., 2008). It is unclear if Jurassic to Cretaceous crustal exhumation of the massifs surrounding the EAB (e.g. Ghorbal et al., 2008) contributed to salt mobilisation and/or led to topographic growth of the anticlines, thereby conditioning former fluvial pathways delivering sediments from the Meseta, High Atlas, and Anti-Atlas domains.

This paper constrains timing and evolution of salt-cored anticlines in the Western High Atlas and discusses whether onshore sediment pathways and offshore sediment distribution are controlled by the topographic expression of those anticlines. We present a workflow to gather geological, structural and stratigraphical data remotely, and to derive cross-sections that are palinspastically restored. We use the workflow to track the topographic grow of two salt-cored anticlines in NW Africa and discuss how it influences nearby sedimentary pathways. Results allow us to compare the time of salt mobilization in the onshore, in the offshore and in the

Central High Atlas basin, and thus, the discussion on potential links with the vertical motions across the Moroccan passive margin.

Geological setting

The Western High Atlas connects the High Atlas fold belt, a Triassic-Jurassic rift basin of the Tethys, and the Atlantic passive margin (Fig. 1; Michard, 2008; Teixell et al., 2003). Terrestrial Triassic rocks are mainly exposed in a 2500 to 5000 m thick sequence in the Argana Valley (Fig. 1b) (Brown, 1980; Ellero et al., 2012; Pique et al., 2002). Intercalated in the Triassic rocks, two tholeiitic basalt flows of the Central Atlantic Magmatic Province (CAMP) yield absolute ages of ~201 Ma (Michard et al., 2008). Intercalated or deposited on top of this sequence, evaporites in variable amounts outcrop along the margin (Hafid, 2000; Hafid et al., 2006; Tari and Jabour, 2013; Fig. 1a). Thickness changes are attributed to the initial configuration of the salt-bearing sub-basins, as dictated by pre-rift basement structures (Tari and Jabour, 2013). Salt deposition occurred on top of coastal syn-rift sedimentary sequences in half-grabens or laterally to them (Hafid et al., 2006; Tari et al., 2013), and evaporites of Lias (Lower Jurassic) age are documented in the Anklout and Imouzzer anticline (Ambroggi, 1963).

The Mesozoic sedimentary record exposed in the Western High Atlas is arguably one of the most complete and fully exposed of NW Africa (e.g. Hafid et al., 2000, Luber, 2017; Duval-Arnould, 2019). The thickness of syn- and post-rift Mesozoic sequences reaches up to c. 7 km in the EAB onshore (Ellouz et al., 2003; Zühlke et al., 2004; Tari and Jabour, 2013; Luber, 2017; Duval-Arnould, 2019) and large-scale anticlines formed by salt diapirism are imaged in the EAB offshore (e.g., Hafid et al., 2006; Pichel et al., 2019; Figs. 1b and 1c).

The Africa-Europe collision forced the Alpine inversion since Late Cretaceous (Hafid et al., 2006). NNW-SSE-directed shortening led to the reactivation of Mesozoic normal faults and forced buckling of both pre-Mesozoic basement and its sedimentary cover, ultimately resulting in the thick-skinned thrusting and folding (Teixell et al., 2003). The Alpine compressional phase overprinted salt-cored anticlines, thereby hindering our capacity to infer salt mobility during the Mesozoic (Michard et al, 2008).

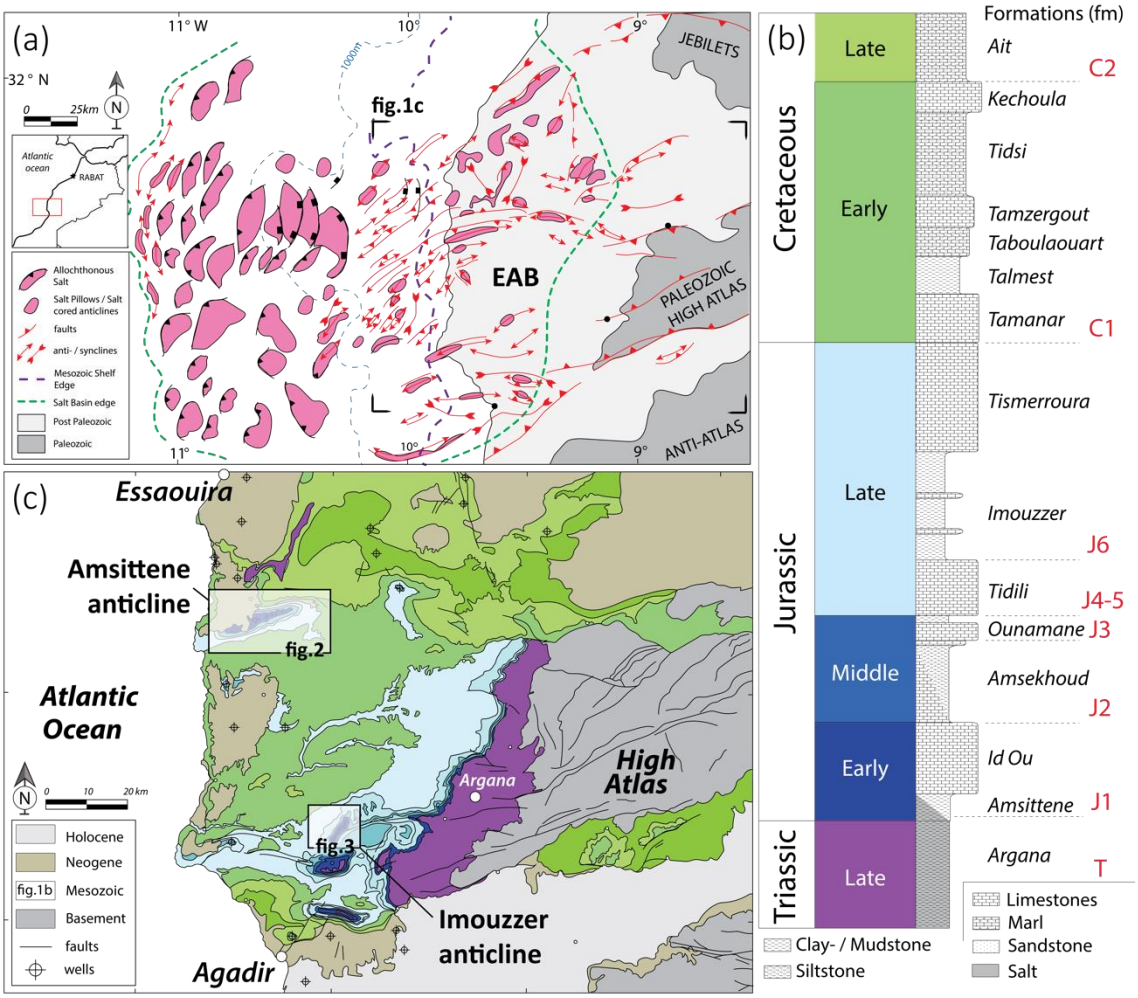

Figure 1 | a) Map of salt structures in the Agadir-Essaouira Basin (EAB) in relation with faults and folds (after Tari et al., 2012). b) Simplified Mesozoic litho-stratigraphic column (after Choubert, 1957, Michard et al., 2008; Duval-Arnould, 2019). c) Geological map of the area (after Hollard et al., 1985).

Material and methods

We map the attitude of geologic horizons and markers, and define their geospatial position, using Google Earth alongside satellite images from the Shuttle Radar Topographic Mission (STRM) and its Digital Elevation Model (DEM), of 90 m spatial resolution and c. 16 m vertical error (Hofmann and Winde, 2010; Rusli et al., 2014). We measure dip angles and azimuths of geologic horizons and markers at km-scale using a 3D plane-solver Google Earth plugin, developed by J. Jamieson and G. Herman and now interrupted (see http:// www.impacttectonics.org/ GeoTools/3pphelp.html). Stratigraphic markers are defined on remote sensing images on the basis of colour changes and 1:50,000 geological maps (e.g., Jaidi et al., 1970). To check the quality of this data set and complement it, we took field measurements (contact coordinates and attitudes) in both anticlines studied (see appendices A and B). Measurements obtained digitally and in the field differ by less than ~10 %. It should also be noted that the DEM in Google Earth is not always accurate for steep slopes (Richard and Ogba, 2016).

We test the geometrical consistency of structural cross-sections using palinspastic restorations. This method reduces uncertainties (Dahlstrom, 1969; Elliot, 1983; Mitra and Namson, 1989; Durand-Riard et al., 2009) and/or allows discrimination between diapirism and shortening (Fahmi et al., 2013). This study preserves the thickness of marine-dominated rocks and uses flexural slip unfolding (Moretti, 2008) to rotate fold limbs to a horizontal datum or an assumed regional surface. Flexural slip is removed during rotation of fold limbs by layer-parallel shear and according to a defined fold axes. During flexural slip unfolding, line length is preserved and true bed thickness is constant, leading fold area conservation in the unfolding direction (Moretti, 2008).

Thickness changes along the anticlines

Amsittene

The ENE-WSW-striking Amsittene Anticline is a c. 40 km-long asymmetric fault-propagation fold (Fernández-Blanco et al., 2020 EarthArXiv; Fig. 2). The Oxfordian beds in the fold northern flank are overturned in the west of the fold, with S-SE dips up to 40°, and dip 20°-30° to the N-NW in the east of the structure. Constant dip angles of 25 to 30° S-SE along the southern flank yield an axial plane that dips c. 85° towards the SSE. Halokinetic effects are only observed in the west of the anticline, where an intrusive Triassic salt outcrops leads Jurassic layers to dip away from it. Thickness variations from the Lias (Sinnemurian-Toarcian) to the Tithonian along a NW-to-SW band show an overall thickness decrease from the northern flank towards the east (Fig. 2d).

In the southern limb, all formations progressively increase in thickness to the west. The Callovian, the Oxfordian and the Kimmeridgian, with thicknesses of c. 50 m, c. 140 m and c. 80 m in the east of the structure, thicken westward along the southern limb to 140 to 200 m, over 300 m and c. 100 m, respectively. The clastic of the Dogger (Aalenian-Bathonian) and Callovian horizons show stronger thinning than younger formations (appendix C). Profiles A and B show northward thickening for all horizons, when restored to the Oxfordian (Fig. 2a). We recover a tectonic shortening of 10-15% along the same direction (Fig. 4) that is consistent with previous estimates (Fernández-Blanco et al., 2020 EarthArXiv).

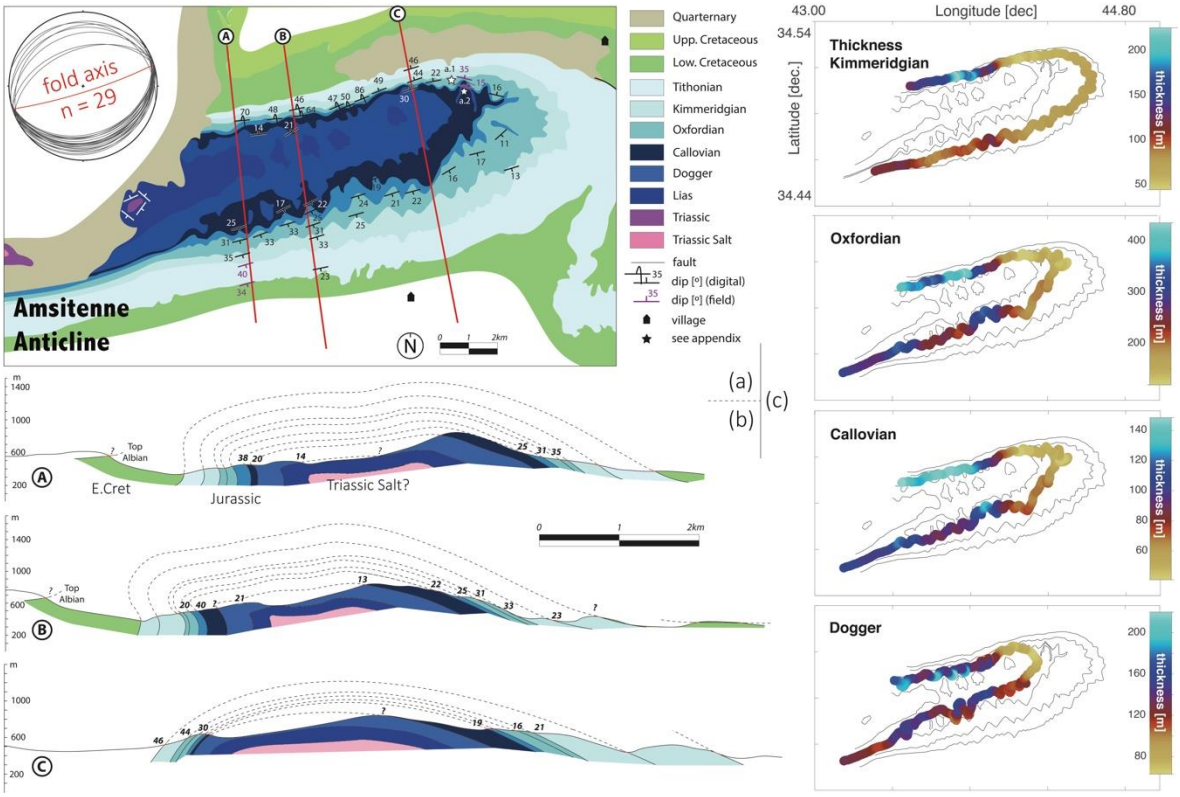

Figure 2 | a) Geological map of the Amsittene Anticline based on Google Earth mapping. See the appendix A for dip measurements. b) Cross-sections A, B, and C, running perpendicular to the fold axis. c) Resulting thickness maps for Middle and Upper Jurassic horizons using the Paradigm Gocad® 'kine3d-1' tool. The resolution of the thickness maps suggests a precision of around 20 m and lies below the thinnest formations modelled in the anticline.

Imouzzer

The NE-SW-striking Imouzzer anticline is c. 15 km long with a hinge line plunging SE (Fig. 3). Jurassic and Cretaceous rocks are folded asymmetrically and no Triassic salt outcrops at the fold core. Syn-sedimentary onlap structures, normal faulting and asymmetric sedimentary thinning suggest active salt diapirism during the Dogger, Callovian and the rest of the Jurassic to Early Cretaceous times (see appendix B). Thicknesses in the Dogger vary slightly along the anticline axis and range from c. 150 to 330 m (Fig. 3c). Thickness variations occur in relation to salts (see Fig. 3 and appendix B for field locations). The thickness of Callovian rocks average 80 m and remains relatively constant throughout the profiles, except for thickening near salt outcrops. Thus, this horizon does not follow thickness trends observed for the Dogger (Fig. 3c). No thickness variation was calculated for Oxfordian and Kimmeridgian units since their data points are too far apart to provide meaningful results, but contain siliciclastic material (appendix C). Results of the structural geometry show a clear difference in the deformation on the Lias unit, especially when compared to that of the Dogger (Fig. 3c). This suggest that Oxfordian rocks were deposited horizontally atop an inherited Liassic anticline. Restoration of NW-SE cross-sections show that shortening varies between ~9 to 6% (Fig. 4).

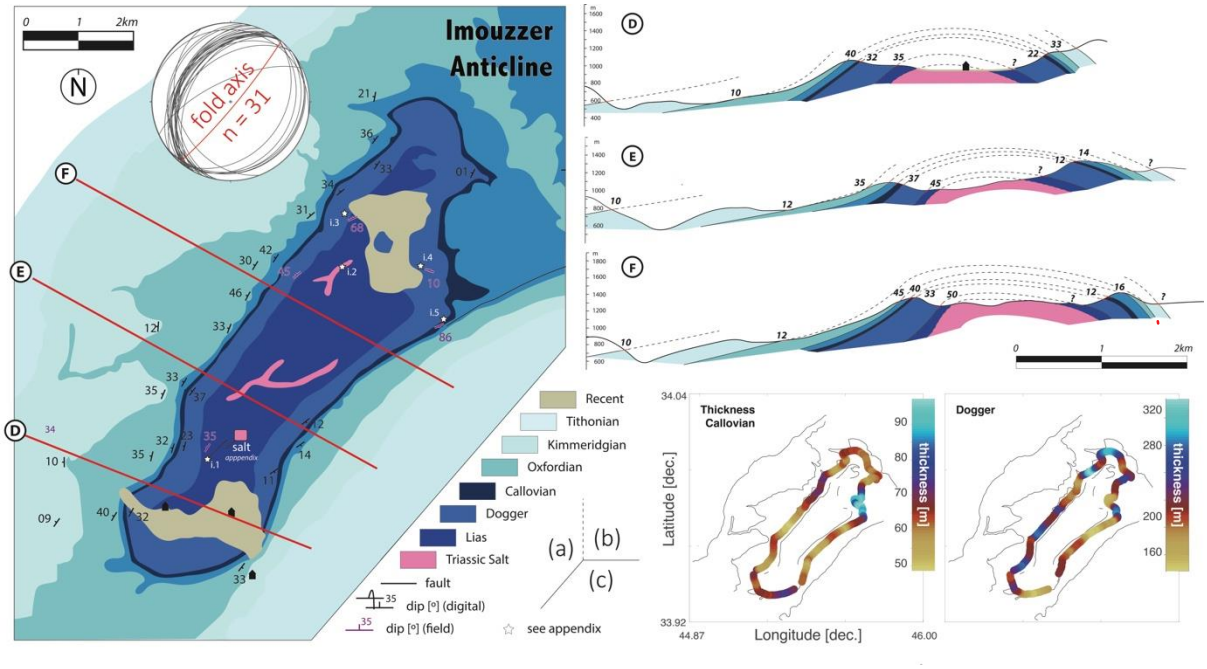

Figure 3 | a) Geological map of the Imouzzer Anticline based on Google Earth mapping. See the appendix B for dip measurements. b) Cross-sections D, E, and F, running perpendicular to the fold axis. C) Resulting thickness maps for Dogger and Callovian horizons using the Paradigm Gocad® 'kine3d-1' tool.

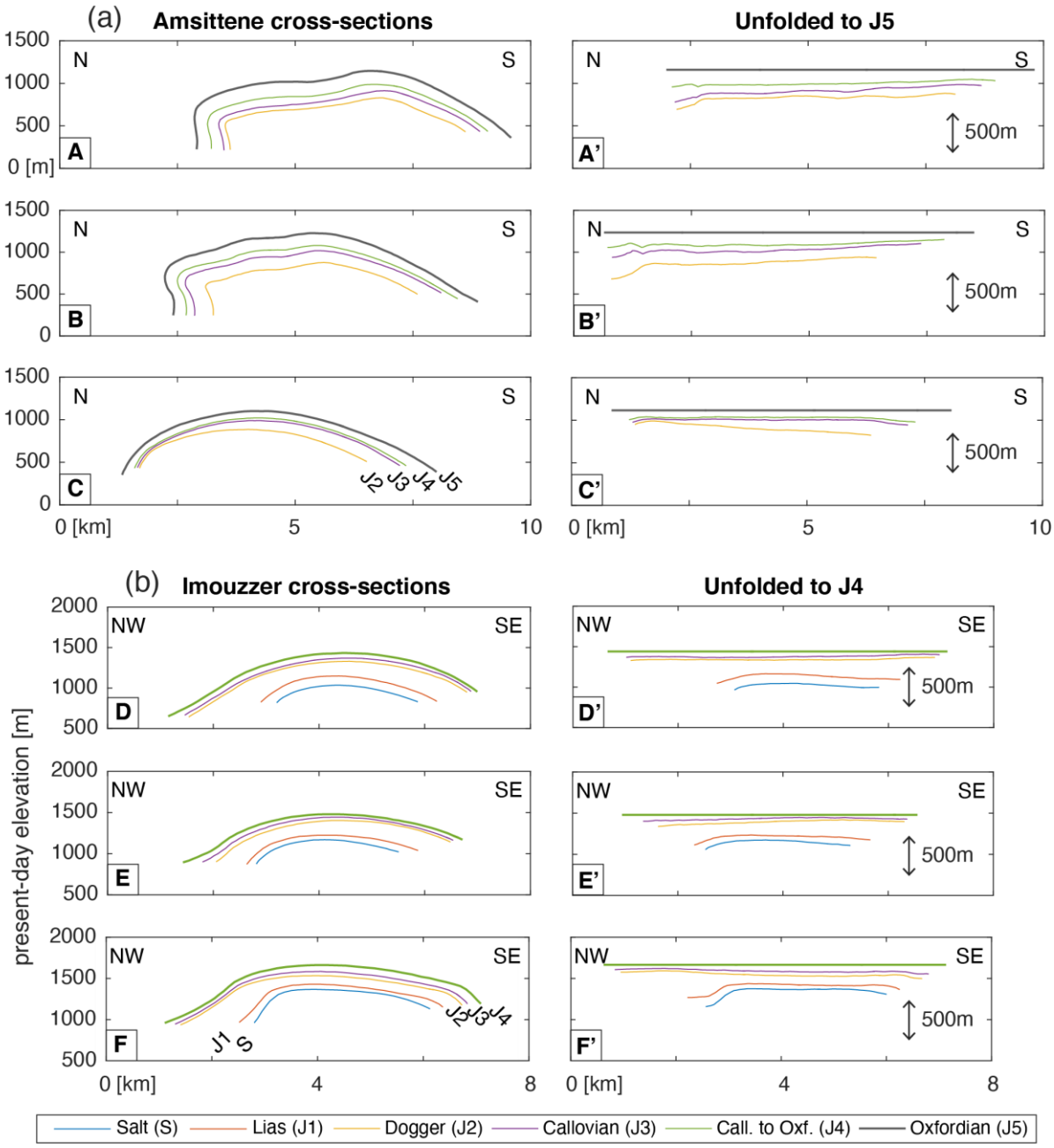

Figure 4 | Cross-sections and restauration to the Oxfordian (J5-4; top of the stratigraphic units) using 2D Move® for a) Amsittene and b) Imouzzer anticlines.

Implications and discussions

Salt mobilisation

Our results suggest Triassic evaporites were mobile in both anticlines from Early to Middle Jurassic (Fig. 5) and that salts were sealed by Late Jurassic carbonates with systematic N-S and E-W thickness variations (Figs. 2 and 3). In the Amsitenne anticline, salt mobilisation occurs in Early to Middle Jurassic (Fig. 5a), and in the Imouzzer anticline (Fig. 5b) the Liassic salt formed a bulge during the Lias and Dogger (Fig. 6a), which strongly deformed the two sedimentary units and possibly led to crestal erosion.

Rock thickness that increase away from the fold axis and nearby salt bodies suggest topographic growth in the sea surface, possibly aided by syn-sedimentary extensional faults (see figures A and B2 of the appendices A and B). In the Agadir-Essaouira Basin (EAB), folds expressed on the sea-floor led to the formation of large carbonate reefs and reef foresets (Fig. 6a; Duval-Arnould, 2019). Relatively-thin evaporites of Toarcian age interbedded in carbonate layers are in good agreement with the observations of thin salts causing structures dominated by thrusts and narrow box-fold anticlines (Hudec and Jackson, 2007). The chaotic patterns of salt deformation in the Imouzzer anticline (see figure B1 of appendix B), suggests salt mobility shortly after deposition.

Early and Middle Jurassic salt mobilisation in the Central High Atlas has been inferred from sedimentary onlaps described by Saura et al. (2014) and later reviewed in Moragas et al. (2018). While the salt mechanisms in the offshore EAB may differ are from those onshore, timing of early salt mobilisation is similar (Neumaier et al., 2015; Pichel et al., 2019; Fig. 6b).

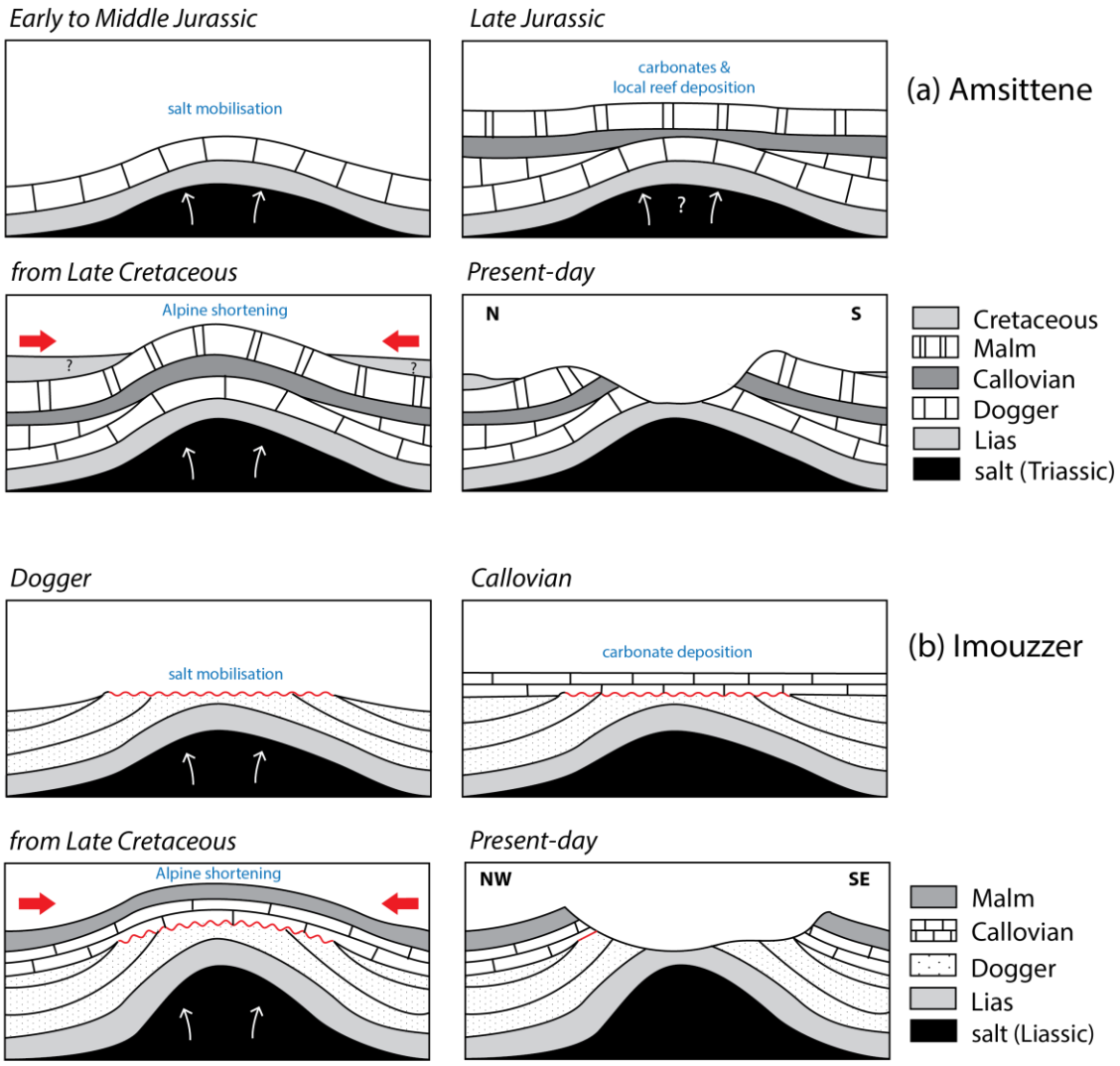

Figure 5 | Conceptual model for the evolution of the a) Amsittene and b) Imouzzer anticlines since the Middle Jurassic (Dogger).

Mechanisms

Salt deformation is unlikely to develop roofs several hundred meters thick, like those shown here, without a component of regional strain (Hudec and Jackson, 2007). Thus, we favour tectonic-induced salt diapirism (Bertotti and Gouiza, 2012; Pique et al., 1998; Stets, 1992). Regional shortening is suggested for the Tidsi and Amsittene anticlines (Bertotti and Gouiza, 2012; Fernández-Blanco et al., 2020 EarthArXiv) to explain structures, syn-sedimentary deformation and the Middle Jurassic to Early Cretaceous exhumation in the EAB.

During the Jurassic, coeval vertical motions of opposite sense resulted in burial of the EAB (e.g., Bertotti and Gouiza, 2012) and erosional exhumation of surrounding massifs (Fig. 6b; e.g., Ghorbal, 2009; Gouiza et al., 2017), thereby leading to a gradient in topography (assuming exhumation is linked to uplift), and possibly a hydraulic head within the Triassic salts. Consequent salt lateral flow in the EAB initiated the concomitant Jurassic folding and the migration of salt diapirs distally from east to west (Hafid et al., 2006; Tari and Jabour, 2013) and led to thickening of Jurassic successions towards the south-west, from near zero in the Argana Valley to ~1 km in the continental shelf break (Zühlke et al., 2004). The Cretaceous series similarly thickens westward, from ~750 m east of the EAB to ~2.5 km (Zühlke et al., 2004). Westward thickening of Mesozoic successions corroborates a westward slope that may thus have led to lateral salt mobility and fold growth.

Alternatively, salt mobilisation may be due to thermal loading (Hudec and Jackson, 2007), induced by the extensive magmatic activity in the Late Triassic (Central Atlantic Magmatic Province; e.g., Davies et al., 2017), or by reactivation of ~NE-SW basement normal faults (e.g., Hafid, 2000; Pique et al., 2001), as described for the offshore areas (Neumaier et al., 2015).

Relations with source-to-sink systems

Transport, sediment channelling and depocenter location (Fig. 6a) are likely the result from the surficial expression of folding and other paleo-topography in the EAB (Fig. 7). Kilometre-scale erosional exhumation occurs in the Meseta and High Atlas during Middle Jurassic to Early Cretaceous and in the Anti-Atlas during Triassic to Middle Jurassic and Late Cretaceous (Fig. 6b; Charton, 2018). Sediment transportation and temporary sinks developed in the EAB with a persistent westward paleo-flow direction in Early Jurassic (Appendix C; Domenech et al., 2018), Middle and Late Jurassic (Ambroggi, 1963; Stets, 1992), and Cretaceous (Essafraoui et al., 2015; Luber, 2017).

Middle Jurassic-Early Cretaceous salt mobility (Fig. 6), marked by thickness variations in up to 10 km wide mini-basins, suggests deep-water fans may have forced differential loading, thus expelling the salts (Fig. 7). Most eroded material deposits over the rifted margin, south of offshore EAB (Agadir segment; Pichel et al., 2019). There, turbiditic deep-water fans likely deposited in the Middle Jurassic and Early Cretaceous (Fig. 7b and 7c; Lancelot and Winterer, 1980; Tari et al., 2012). Early Cretaceous fluvial systems sourcing detritus and leading to a sedimentary succession of c. 7 km atop the Triassic salt (Pichel et al., 2019) are preserved and exposed in the onshore EAB (Luber, 2017; Luber et al., 2019).

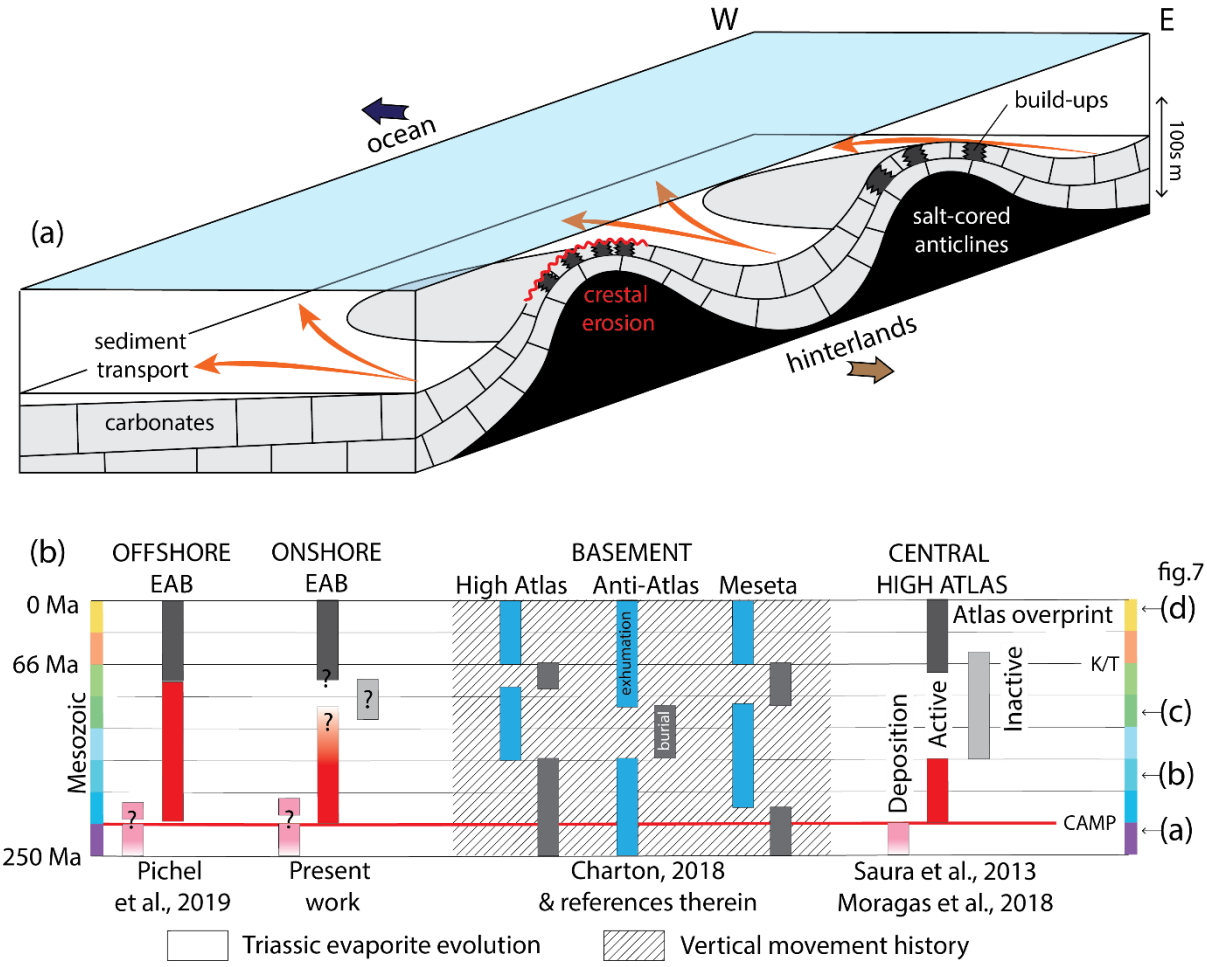

Figure 6 | a) Highly idealized channelization of sediment transport in a shallow marine environment and b) timing of salt mobilization and exhumation in surrounding massifs.

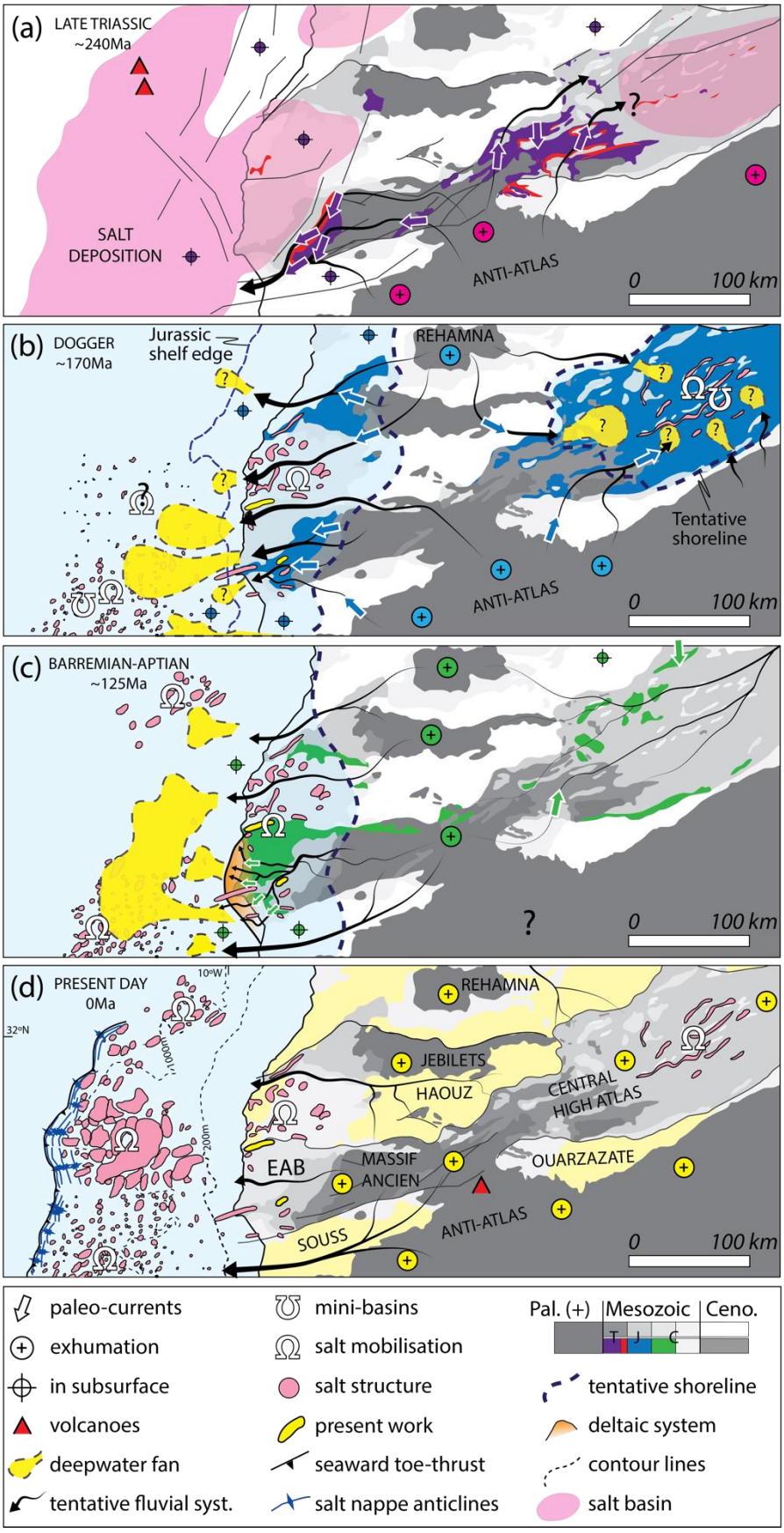
(a) LATE TRIASSIC
~240Ma
SALT
DEPOSITION
ANTI-ATLAS
0
100 km
(b) DOGGER
~170Ma
Jurassic
shelf edge
REHAMNA
Tentative
shoreline
ANTI-ATLAS
0
100 km
(c) BARREMIAN-APTIAN
~125Ma
0
100 km
(d) PRESENT DAY
0Ma
10°W
32°N
REHAMNA
JEBILETS
HAOUZ
CENTRAL
HIGH ATLAS
EAB
MASSIF
ANCIEN
OUARZAZATE
SOUSS
ANTI-ATLAS
0
100 km
paleo-currents
exhumation
in subsurface
volcanoes
deepwater fan
tentative fluvial syst.
mini-basins
salt mobilisation
salt structure
present work
seaward toe-thrust
salt nappe anticlines
Pal. (+)
Mesozoic
Ceno.
T
J
C
tentative shoreline
deltaic system
contour lines
salt basin

Figure 7 | Tentative paleo-reconstructions of the EAB and surrounding massifs (made from the compilations of paleogeography, depositional environment, and structural maps; see references below) during four selected times (Fig. 6b). Exhumation, presence in subsurface, and tentative shoreline after Charton (2018). Salt structures outlined in the offshore of the EAB and High Atlas after Michard et al. (2008), Hafid et al. (2010), and Moragas et al. (2017). Timing of salt mobilization after Figure 6b and references therein. a) Late Triassic. Salt basin outlines after Pichel et al. (2019) and Tari et al. (2013), paleocurrents after Brown (1980), Courel et al. (2003), and Mader (2005), and paleo-reconstruction after Domenech et al. (2018); b) Middle Jurassic. Tentative shoreline after Charton (2018), paleocurrents after Stets (1992), and paleo-reconstruction after Nemcok et al. (2005) and Tari et al. (2013). c) Barremian-Aptian. Tentative shoreline after Charton (2018), paleocurrents after Luber (2017), Cavallina et al. (2018), Haddoumi et al. (2018), and paleo-reconstruction after ONHYM (2004), Nemcok et al. (2005) and Tari et al. (2013). d) Present-day situation.

Conclusions

This study shed new light into the controversial question about whether salt-cored folds in the EAB are shaped by Cenozoic compressional forces or Mesozoic salt diapirism. The results show that salt mobilisation was already active during the Early to Middle Jurassic and, therefore, before the Atlasic orogeny. Mobilisation of Triassic and Liassic salt layers was most likely initiated by Jurassic exhumation patterns in the hinterland and subsidence towards the offshore, causing a hydraulic head gradient that led to lateral salt flow. Another possible scenario is a period of regional shortening in the Jurassic, similar to what was postulated in previous studies, but no supporting evidence could be added from the present work.

As a consequence of early fold growth, the anticlines controlled the sediment pathways of eroded material, coming from the exhumed Variscan massifs in the hinterland, being shed towards the present-day offshore basin. We submit that the location of depocenters (deep-sea fans) of Jurassic to Early Cretaceous age are therefore dependent on the location of the salt-cored anticlines in the EAB.

References

Ambroggi, R., 1963. Etude géologique du versant méridional du Haut Atlas occidental et de la plaine du Souss. Editions du Service géologique du Maroc.

Bertotti, G. and Gouiza, M., 2012. Post-rift vertical movements and horizontal deformations in the eastern margin of the Central Atlantic: Middle Jurassic to Early Cretaceous evolution of Morocco. International Journal of Earth Sciences, 101, pp.2151-2165.

Brown, R.H., 1980. Triassic rocks of Argana Valley, southern Morocco, and their regional structural implications. AAPG Bulletin, 64, pp.988-1003.

Cavallina, C., Papini, M., Moratti, G. and Benvenuti, M., 2018. The late Mesozoic evolution of the Central High Atlas domain (Morocco): Evidence from the paleo-drainage record of the Adrar Aglagal syncline. Sedimentary Geology, 376, pp.1-17.

Charton, R., 2018. Phanerozoic Vertical Movements in Morocco. Doctoral dissertation, Delft University of Technology, 165 pp.

Choubert, G., 1957. Carte géologique du Maroc au 1/500.000, feuille Marrakech. Notes et Mémoires du Service géologique du Maroc, 70.

Courel, L., Salem, H.A., Benaouiss, N., Et-Touhami, M., Fekirine, B., Oujidi, M., Soussi, M. and Tourani, A., 2003. Mid-Triassic to Early Liassic clastic/evaporitic deposits over the Maghreb Platform. Palaeogeography, Palaeoclimatology, Palaeoecology, 196, pp.157-176.

Domenech, M., 2015. Rift opening and inversion in the Marrakech High Atlas: integrated structural and thermochronologic study: Universitat Autònoma de Barcelona, Ph.D. Thesis, 157 p.

Dahlstrom, C. D. A., 1969. Balanced cross sections, Can. J. Earth Sci., 6, p. 743–757.

Davies, J.H.F.L., Marzoli, A., Bertrand, H., Youbi, N., Ernesto, M. and Schaltegger, U., 2017. End-Triassic mass extinction started by intrusive CAMP activity. Nature communications, 8, pp.1-8.

Domènech, M., Stockli, D. and Teixell, A., 2018. Detrital zircon U-Pb provenance and paleogeography of Triassic rift basins in the Marrakech High Atlas: Terra Nova, 30, p. 310-318. doi:10.1111/ter.12340

Durand-Riard, P., Caumon, G. and Muron, P., 2010. Balanced restoration of geological volumes with relaxed meshing constraints. Computers & Geosciences, 36, pp.441-452.

Duval-Arnould A.,2019.. Controls on stratigraphic development of shelf margin carbonates: Jurassic Atlantic margin – Essaouira-Agadir Basin, Western Morocco : PhD Thesis, University of Manchester, 287p.

Ellero, A., Ottria, G., Malusà, M.G. and Ouanaimi, H., 2012. Structural geological analysis of the High Atlas (Morocco): evidences of a transpressional fold-thrust belt. Tectonics-Recent Advances.

Elliot, D., 1983. The construction of balanced cross-section. Journal of Structural Geology, 5.

Ellouz, N., Patriat, M., Gaulier, J.-M., Bouatmani, R. and Sabounji, S.,2003.. From rifting to Alpine inversion: Mesozoic and Cenozoic subsidence history of some Moroccan basins: Sedimentary Geology, 156, p. 185–212. doi:10.1016/S0037-0738(02.00288-9

Essafraoui, B., Ferry, S., Groshény, D., Içame, N., El Aouli, H., Masrour, M., Bulot, L.G., Géraud, Y. and Aoutem, M., 2015. Sequence stratigraphic architecture of marine to fluvial deposits across a passive margin (Cenomanian, Atlantic margin, Morocco, Agadir transect). Carnets de géologie.

Fahmi, M.A., Plesch, A., Shaw, J., and Cole, J., 2013. Evolution of structures above a salt diapir - case study from the arabian gulf region. AAPG Annual Convention and Exhibition

Fernández-Blanco, D., Gouiza, M., Charton, R. J., Kluge, C., Klaver, J., Brautigam, K., & Bertotti, G. 2020 (preprint of 2019, January 10). Anticline growth by shortening during crustal exhumation of the Moroccan Atlantic margin. In review.

Frizon de Lamotte, D., Leturmy, P., Missenard, Y., Khomsi, S., Ruiz, G., Saddiqi, O., Guillocheau, F. and Michard, A.,2009.. Mesozoic and Cenozoic vertical movements in the Atlas system (Algeria, Morocco, Tunisia.: An overview: Tectonophysics, 475, p. 9–28. doi:10.1016/j.tecto.2008.10.024

Ghorbal, B.,2009.. Mesozoic to Quaternary thermo-tectonic evolution of Morocco (NW Africa.: Vrije Universiteit Amsterdam, Ph.D. Thesis, 226 p.

Ghorbal, B., Bertotti, G., Foeken, J. and Andriessen, P.,2008.. Unexpected Jurassic to Neogene vertical movements in 'stable' parts of NW Africa revealed by low temperature geochronology: Terra Nova, 20, p. 355–363. doi:10.1111/j.1365-3121.2008.00828.x

Gouiza, M., Charton, R., Bertotti, G., Andriessen, P. and Storms, J.E.A., 2017. Post-Variscan evolution of the Anti-Atlas belt of Morocco constrained from low-temperature geochronology. International Journal of Earth Sciences, 106, pp.593-616.

Haddoumi, H., Charrière, A., Feist, M., Baidder, L., Ferrière, J., Karim, M., Ettachfini, E.M., Mamoun, S.M., Chennouf, R., Rachdi, A. and Adardor, S., 2019. A Barremian-? Aptian Tethyan precursor of the Cretaceous marine flooding of Morocco: Evidence from the red-bed series within the "Marginal Folds" of the eastern High Atlas. Cretaceous Research, 95, pp.37-60.

Hafid, M., 2000. Triassic–early Liassic extensional systems and their Tertiary inversion, Essaouira Basin (Morocco). Marine and Petroleum Geology, 17, pp.409-429.

Hafid, M., Salem, A.A. and Bally, A.W., 2000. The western termination of the Jebilet–high Atlas system (offshore Essaouira Basin, Morocco). Marine and Petroleum Geology, 17, pp.431-443.

Hafid, M., Tari, G., Bouhadioui, D., El Moussaid, I., Echarfaoui, H., Salem, A.A., Nahim, M. and Dakki, M., 2008. Atlantic basins. In Continental evolution: The geology of Morocco (pp. 303-329). Springer, Berlin, Heidelberg.

Hafid, M., Zizi, M., Bally, A.W. and Ait Salem, A.,2006.. Structural styles of the western onshore and offshore termination of the High Atlas, Morocco: Comptes Rendus Geoscience, 338, p. 50–64. doi:10.1016/j.crte.2005.10.007

Hoffmann, E. and Winde, F., 2010. Generating high-resolution digital elevation models for wetland research using Google EarthTM imagery: an example from South Africa. Water SA, 36, pp.53-68.

Hollard, H., Choubert, G., Bronner, G., Marchand, J. and Sougy, J., 1985. Carte géologique du Maroc, scale 1: 1,000,000. Serv. Carte géol. Maroc, 260(2).

Hudec, M.R. and Jackson, M.P., 2007. Terra infirma: Understanding salt tectonics. Earth-Science Reviews, 82, pp.1-28.

Jaidi, S.E.M., Bencheqroun, A., Diouri, M. and Ennadifi, Y., 1970. Carte Géologique de l'Anti-Atlas central et de la zone synclinale de Ouarzazate 1: 200 000, Feuilles Ouarzazate, Alougoum et Telouet Sud. Not. Mém. Serv. Géol. Maroc, 138.

Lancelot, Y. and Winterer, E.L., 1980. Evolution of the Moroccan oceanic basin and adjacent continental margin—a synthesis. Initial Reports of the Deep Sea drilling project, 50, pp.801-821.

Luber, T., 2017. Integrated Analysis of Lower Cretaceous Stratigraphy and depositional systems: The Essaouira-Agadir basin of Morocco: University of Manchester, Ph.D. Thesis, 257 p.

Luber, T.L., Bulot, L.G., Redfern, J., Nahim, M., Jeremiah, J., Simmons, M., Bodin, S., Frau, C., Bidgood, M. and Masrour, M., 2019. A revised chronostratigraphic framework for the Aptian of the Essaouira-Agadir Basin, a candidate type section for the NW African Atlantic Margin. Cretaceous Research, 93, pp.292-317.

Mader, N.K., 2005. Sedimentology and sediment distribution of Upper Triassic fluvio-aeolian reservoirs on a regional scale (Central Algeria, SW Morocco, NE Canada): an integrated approach unravelling the influence of climate versus tectonics on reservoir architecture (Doctoral dissertation, The University of Manchester (United Kingdom)).

Michard, A., Saddiqi, O., Chalouan, A. and de Lamotte, D.F.,2008.. Continental Evolution: The Geology of Morocco: Springe, 424 p.

Mitra, S. and Namson, J.S., 1989. Equal-area balancing. American Journal of Science, 289, pp.563-599.

Moragas, M. , Vergés, J. , Saura, E. , Martín-Martín, J. , Messager, G. , Merino-Tomé, Ó. , Suárez-Ruiz, I. , Razin, P. , Grélaud, C. , Malaval, M. , Joussiaume, R. and Hunt, D. W.,2018.. Jurassic rifting to post-rift subsidence analysis in the Central High Atlas and its relation to salt diapirism: Basin Research, 30, 336-362. doi:10.1111/bre.12223

Moragas, M., Vergés, J., Nalpas, T., Saura, E., Martín-Martín, J.D., Messager, G. and Hunt, D.W., 2017. The impact of syn-and post-extension prograding sedimentation on the development of salt-related rift basins and their inversion: Clues from analogue modelling. Marine and Petroleum Geology, 88, pp.985-1003.

Moretti, I., 2008. Working in complex areas: New restoration workflow based on quality control, 2D and 3D restorations. Marine and Petroleum Geology, 25, pp.205-218.

Nemčok, M., Stuart, C., Segall, M.P. and Allen, R.B.,2005.. Structural development of southern Morocco: Interaction of tectonics and deposition: Annual Bob F. Perkins Research Conference, 25, Houston p. 151–202.

Neumaier, M., Back, S., Littke, R., Kukla, P.A., Schnabel, M. and Reichert, C., 2016. Late Cretaceous to Cenozoic geodynamic evolution of the Atlantic margin offshore Essaouira (Morocco). Basin Research, 28(5), pp.712-730.

Muniz Pichel, L., 2018. Tectono-stratigraphic evolution associated with salt tectonics along Atlantic margins: effects of pre-salt relief and regional events (Doctoral dissertation, University of Manchester).

Pichel, L.M., Huuse, M., Redfern, J. and Finch, E., 2019. The influence of base-salt relief, rift topography and regional events on salt tectonics offshore Morocco. Marine and Petroleum Geology, 103, pp.87-113.

Piqué, A., Le Roy, P. and Amrhar, M., 1998. Transtensive synsedimentary tectonics associated with ocean opening: the Essaouira–Agadir segment of the Moroccan Atlantic margin. Journal of the Geological Society, 155, pp.913-928.

Pique, A., Tricart, P., Guiraud, R., Laville, E., Bouaziz, S., Amrhar, M., and Ouali, R.A., 2002. The Mesozoic-Cenozoic atlas belt (North Africa): an overview. Geodinamica Acta, 15, pp. 185–202.
Piqué, A. and Carpenter, M.S., 2001. Geology of northwest Africa. Gebrüder Borntraeger, 29.

Richard, J.U. and Ogba, C., 2016. Analysis of Accuracy of Differential Global Positioning System (DGPS) and Google Earth Digital Terrain Model (DTM) Data Using Geographic Information System Techniques. Journal of Geodesy and Geomatics Engineering, 2, pp. 52-61

Rojo, L.A. and Escalona, A., 2018. Controls on minibasin infill in the Nordkapp Basin: Evidence of complex Triassic synsedimentary deposition influenced by salt tectonics. AAPG Bulletin, 102, pp.1239-1272.

Rusli, N., Majid, M.R. and Din, A.H.M., 2014. Google Earth's derived digital elevation model: A comparative assessment with Aster and SRTM data. In IOP Conference Series: Earth and Environmental Science, IOP Publishing, 18, p. 012065.

Saddiqi, O., Haimer, El, F.Z., Michard, A., Barbarand, J., Ruiz, G.M.H., Mansour, E.M., Leturmy, P. and de Lamotte, D.F.,2009.. Apatite fission-track analyses on basement granites from south-western Meseta, Morocco: Paleogeographic implications and interpretation of AFT age discrepancies: Tectonophysics, 475, p. 29–37. doi:10.1016/j.tecto.2009.01.007

Saura, E., Vergés, J., Martín-Martín, J.D., Messager, G., Moragas, M., Razin, P., Grélaud, C., Joussiaume, R., Malaval, M., Homke, S. and Hunt, D.W., 2014. Syn-to post-rift diapirism and minibasins of the Central High Atlas (Morocco): the changing face of a mountain belt. Journal of the Geological Society, 171, pp.97-105.

Stets, J., 1992. Mid-jurassic events in the western high Atlas (Morocco). Geologische Rundschau, 81, pp.69-84.

Tari, G., Hussein, H., Novotny, B., Hannke, K. and Kohazy, R., 2012. Play types of the deep-water Matruh and Herodotus basins, NW Egypt. Petroleum Geoscience, 18, pp.443-455.

Tari, G. and Jabour, H.,2013.. Salt tectonics along the Atlantic margin of Morocco: Geological Society, London, Special Publications, 369, p. 337–353. doi:10.1144/SP369.23

Teixell, A., Arboleya, M.-L., Julivert, M. and Charroud, M.,2003.. Tectonic shortening and topography in the central High Atlas (Morocco.: Tectonics, 22, TC1051. doi:10.1029/2002TC001460

Venus, J.H., Mountney, N.P. and McCaffrey, W.D., 2015. Syn-sedimentary salt diapirism as a control on fluvial-system evolution: an example from the proximal Permian Cutler Group, SE Utah, USA. Basin Research, 27, pp.152-182.Verges et al., 2017

Zühlke, R., Bouaouda, M.S., Ouajhain, B., Bechstädt, T. and Leinfelder, R., 2004. Quantitative Meso-/Cenozoic development of the eastern central Atlantic continental shelf, western High Atlas, Morocco. Marine and Petroleum Geology, 21, pp.225-276.

Acknowledgements

This work is the result of the second author's M.Sc. Thesis. We are grateful to the North Africa Research Group (NARG) for sponsoring field work. Academic licenses of the TUDelft were used for Move 2D and GoCAD.

Appendix

A - Amsitene fieldwork and dip measurements

Figure Aa shows a large normal fault cutting the Oxfordian with a displacement of around 50m (location a.2). The axial plane is dipping 60° to the North. The fault zone is characterised by a cataclasic fault zone and marl smeared out on the fault. The yellow marl, which is also visible on satellite images, is the key feature to determine the style of displacement and to measure the displacement itself. Indications for a compressional stress regime with regional shortening, are given by en-echelon structures, joints, and stylolites, which are not parallel or perpendicular to bedding. They indicate a shortening direction of roughly NE-SW, although joints and stylolites in figure veins indicate two different stress directions, one NW-SE and another one NNE-SSW. The latter seemed to have occurred later in time, since the joints connect pre-existing fractures or veins and do not cross them. Still, these features show that the anticline has previously been involved in two different tectonic shortening events, later than the Callovian.

On the northeastern side of the anticline at location a.1 (Fig. 2), Dogger to Kimmeridgian rocks are exposed. A cliff of almost 15m of carbonate rocks, most likely Dogger to Callovian rocks, shows discontinuous layers forming onlap structures (Fig. Ab and c). Onlaps occur towards the south, i.e. the center of the anticline. These onlaps result in a thickening of more than 5m over a distance of about 50m towards the north (Fig. Ab). This results in a change in dip from 25° in the upper section to 15° in the lower section.

Anticline	Dip	Latitude	Longitude	Formation
Amsittene	13/141	31°10'12.98"N	9°38'49.50"W	Dogger
Amsittene	21/330	31°11'2.55"N	9°39'3.13"W	Dogger
Amsittene	14/345	31°11'1.79"N	9°39'50.24"W	Dogger
Amsittene	25/162	31° 9'21.04"N	9°40'1.25"W	Callovian
Amsittene	17/153	31° 9'42.97"N	9°39'8.18"W	Callovian
Amsittene	22/154	31° 9'48.17"N	9°38'43.17"W	Callovian
Amsittene	19/160	31°10'21.36"N	9°37'24.07"W	Callovian
Amsittene	49/338	31°11'50.50"N	9°37'16.49"W	Callovian
Amsittene	35/158	31°11'31.01"N	9°38'9.03"W	Callovian
Amsittene	40/172	31°11'20.27"N	9°38'58.57"W	Callovian
Amsittene	38/175	31°11'14.68"N	9°39'25.21"W	Callovian
Amsittene	31/166	31° 9'13.83"N	9°40'1.16"W	Oxfordian
Amsittene	35/164	31° 9'6.75"N	9°40'0.69"W	Oxfordian
Amsittene	33/159	31° 9'16.67"N	9°39'38.29"W	Oxfordian
Amsittene	33/164	31° 9'29.10"N	9°39'2.00"W	Oxfordian
Amsittene	31/161	31° 9'31.49"N	9°38'40.04"W	Oxfordian
Amsittene	25/155	31° 9'38.76"N	9°38'40.09"W	Oxfordian
Amsittene	28/162	31° 9'42.55"N	9°38'10.42"W	Oxfordian
Amsittene	25/164	31° 9'52.55"N	9°37'44.84"W	Oxfordian
Amsittene	24/163	31°10'3.79"N	9°37'43.59"W	Oxfordian
Amsittene	21/162	31°10'2.99"N	9°37'2.68"W	Oxfordian
Amsittene	22/165	31°10'6.12"N	9°36'37.80"W	Oxfordian
Amsittene	16/149	31°10'29.44"N	9°35'57.46"W	Oxfordian
Amsittene	17/166	31°10'41.37"N	9°35'27.35"W	Oxfordian
Amsittene	11/138	31°11'6.28"N	9°34'53.53"W	Oxfordian
Amsittene	16/013	31°11'49.96"N	9°35'2.30"W	Oxfordian
Amsittene	22/349	31°12'0.19"N	9°36'18.47"W	Oxfordian
Amsittene	32/161	31°11'34.60"N	9°37'59.99"W	Oxfordian
Amsittene	22/189	31°11'26.61"N	9°38'25.40"W	Oxfordian
Amsittene	23/168	31° 9'1.86"N	9°38'34.36"W	Tithonian
Amsittene	46/343	31°12'8.85"N	9°36'43.62"W	Tithonian
Amsittene	13/163	31°10'29.50"N	9°34'48.66"W	Kimmeridgian
Amsittene	33/163	31° 9'21.01"N	9°38'37.96"W	Kimmeridgian

Table A | Google Earth and field dip measurements of the Amsittene anticline

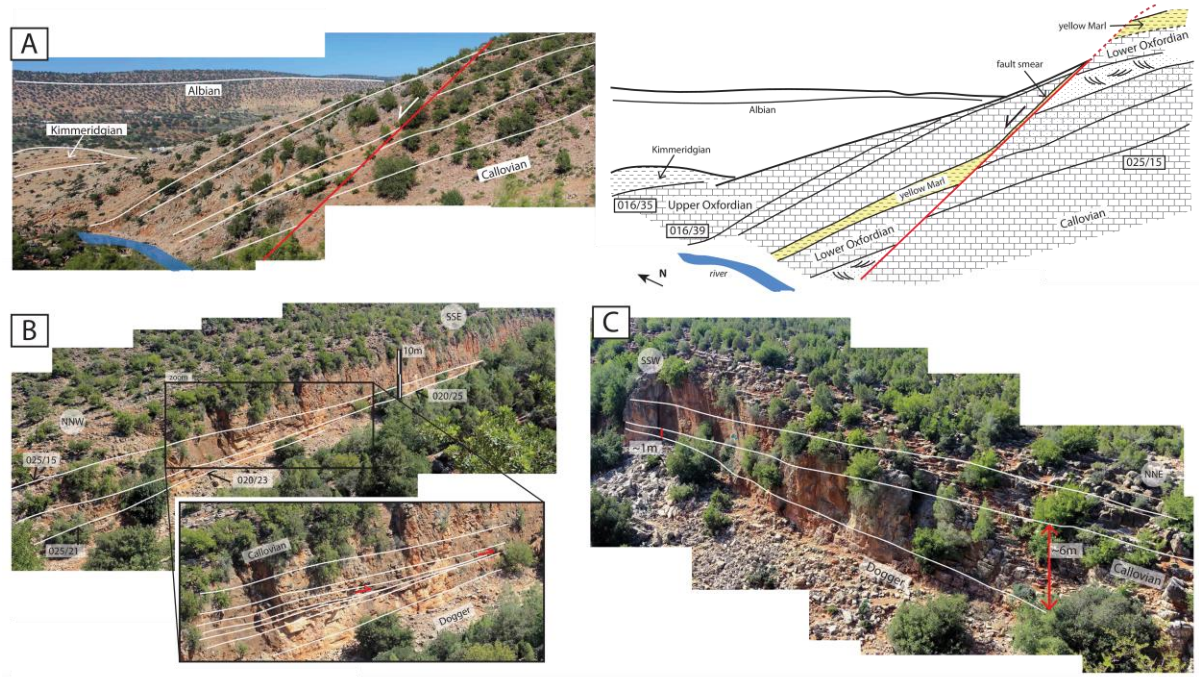

Figure A | a) Normal faulting and b-c) syn-sedimentary onlap structures in the Dogger to Callovian.

B - Imouzzer: fieldwork and dip measurements

Thick layers of salt (gypsum) are interbedded in carbonate layers of the Lias (Fig. B1). Salt layers are dipping NE following the morphology of the fold core. Deformation of the carbonate layers interbedded in the salt are found all along the valley, showing multiple folding structures and diapir intrusions (Fig. B1d). The orientation of the bedding is different from the general trend of NW dipping layers at the western flank. The thickness of the salt can be assumed to amount at least to 50m, since the base of the salt is not visible.

In the Northern part (Fig. B2a), Liassic-Dogger sediments dip 68° NNW, forming a conformable contact. The marly to sandy deposits of the Dogger, with thicknesses of 200 to 250m, are strongly deformed. Folding is observed at the base (Fig. B2b and c), whereas towards the top deformation features are of a faulted nature, showing normal faulting and smaller fold structures (Fig. B2d). Subtle changing thickness of those layers from S to N of a normal fault might indicate syn-sedimentary deformation. The contact from Dogger to Callovian is showing an angular unconformity (Fig. B2a). The contact angle between the two is extrapolated to approximately 30°meaning that the Dogger might have had a structural dip when the Callovian was deposited.

Joints, en-echelon structures and stylolites in Callovian rocks indicate two different shortening directions. The NNE-SSW compressional features can likely be linked to the Alpine shortening. The NW-SE, however, is either a result of an earlier local rotation of the compressional axes within the Alpine orogeny, or pinpoints towards a much earlier compressional event, maybe in the Middle or Later Jurassic, which led to the mobilisation of the salt and an early stage of fold growth.

Anticline	Dip	Latitude	Longitude	Formation
Imouzzer	23/285	30°41'29.78"N	9°29'34.34"W	Dogger
Imouzzer	37/308	30°41'53.71"N	9°29'32.33"W	Dogger
Imouzzer	25/299	30°42'49.88"N	9°28'38.29"W	Dogger
Imouzzer	34/321	30°43'38.48"N	9°28'4.30"W	Dogger
Imouzzer	01/296	30°43'42.21"N	9°26'40.14"W	Dogger
Imouzzer	12/141	30°41'38.33"N	9°28'17.30"W	Dogger
Imouzzer	11/146	30°41'18.29"N	9°28'33.67"W	Dogger
Imouzzer	32/299	30°40'54.58"N	9°30'8.19"W	Dogger
Imouzzer	41/301	30°41'58.99"N	9°29'37.21"W	Oxfordian
Imouzzer	44/306	30°43'4.24"N	9°28'40.20"W	Oxfordian
Imouzzer	36/307	30°43'59.63"N	9°27'44.03"W	Oxfordian
Imouzzer	21/280	30°44'30.93"N	9°27'38.20"W	Oxfordian
Imouzzer	40/301	30°40'53.13"N	9°30'14.12"W	Oxfordian
Imouzzer	33/127	30°40'28.78"N	9°28'53.57"W	Oxfordian
Imouzzer	14/145	30°41'29.56"N	9°28'18.50"W	Oxfordian
Imouzzer	22/122	30°40'37.19"N	9°28'45.83"W	Oxfordian

Table B | Google Earth and field dip measurements of the Amsittene anticline

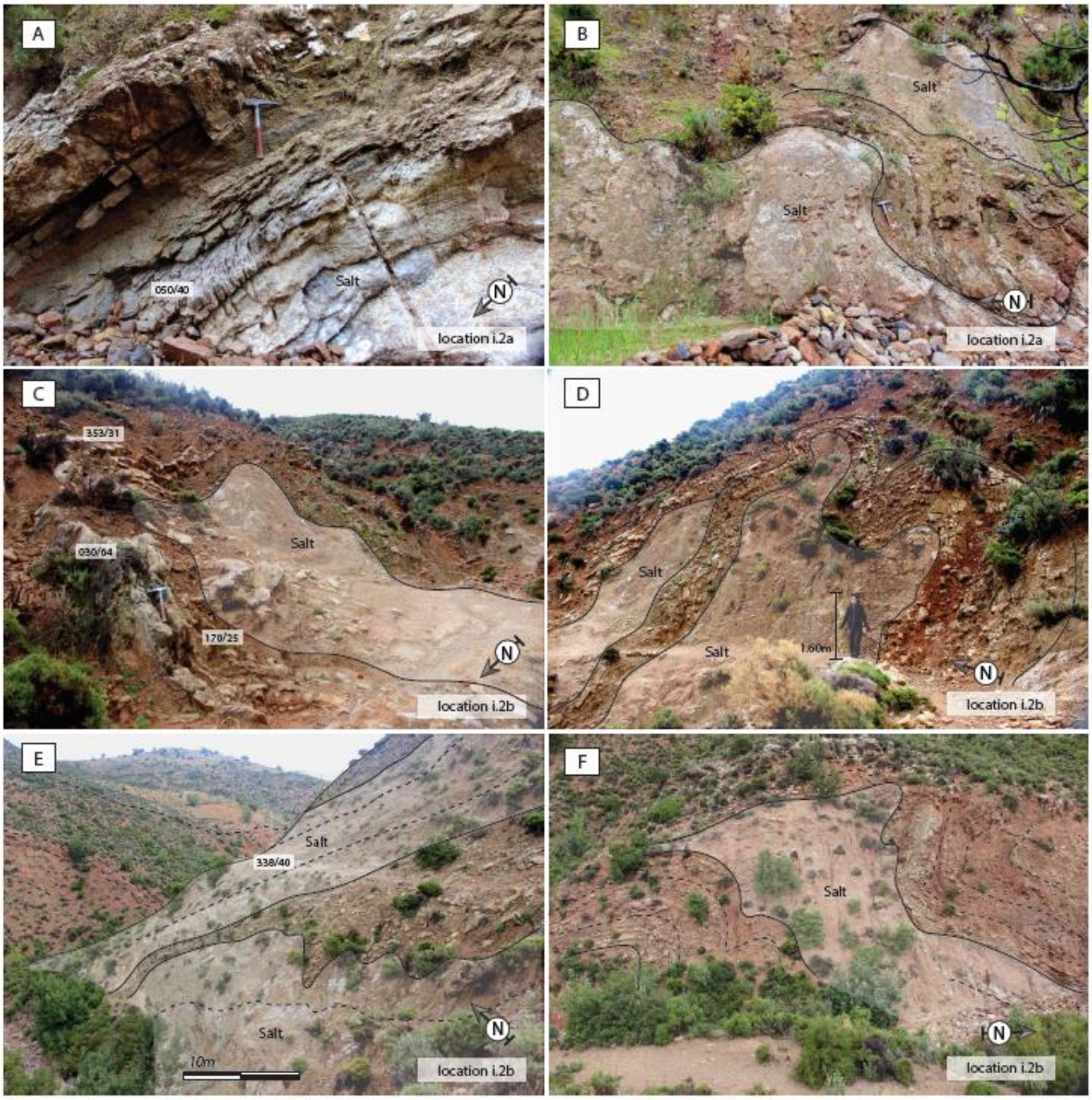

Figure B1 | Pictures of salt in the core of Immouzer anticline and related deformation. See locations on figure 3 of the main text.

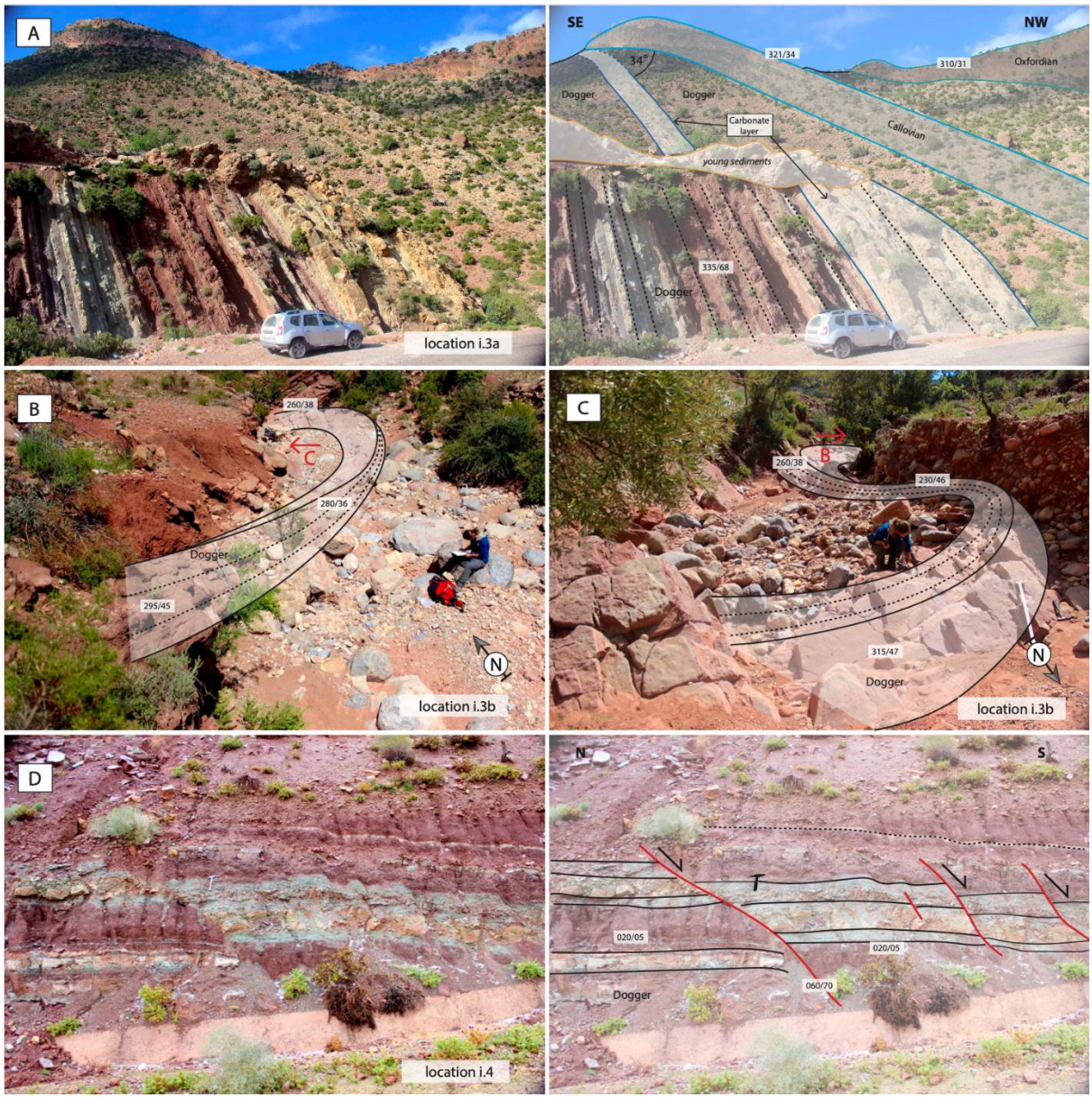

Figure B2 | Dogger showing an angular uncorformity, folding, and normal faulting.

C – Facies variation and siliciclastic influx

Along the Imouzzer and Amsittène anticlines, disparities in term of siliciclastic influx have been recorded (Duval-Arnould, 2019; Fig. C). Along the Imouzzer Anticline, the N-W flank records siliciclastic deposits during the Middle to Upper Orfordian (Fig. C, S2), which are absent along all the eastern flank of the anticline and in the SW part of the anticline. In the Amsittène anticline, the same Oxfordian siliciclastic influx is observable along the northern and southern flanks, but a prior siliciclastic influx (Fig. C, S1), dated Lower to Middle Callovian is also visible along the northern flank of the anticline while absent along the southern flank.

For the Amsittène Anticline, another important sedimentological aspect is the facies variations in the Callovian deposits (Duval-Arnould, 2019). The southern flank Callovian deposits present deeper facies and deeper water fauna (abundant ammonites) compared to the northern flank. This indicates the presence of a topographic high in the northern part of the anticline. Some potential salt movements might have happen prior to the Callovian stage to create this high. The high could also have acted as a barrier to siliciclastic deposits coming from the north, which would have deposited in this shallower domain, and forbade them to reach the other side of the Anticline.

For the Imouzzer Anticline, the north and south of the anticline present fairly similar deposits thicknesses during the Callovian (Duval-Arnould, 2019). The Callovian facies are homogeneous along the anticline and followed by coral build-ups during the Oxfordian. This coral-rich unit is then interrupted in the north of the anticline by cross-bedded siliciclastic deposits. This siliciclastic influx (S2) is not recorded towards the south of the anticline. It takes place at the same stratigraphic position in the Amsittène and Imouzzer anticlines and have been therefore interpreted to be due to the same processes. Everywhere in the basin, a strong regression marks the end of the coral-rich units and the transition to shallow water, tidal-flat deposits.

The deposition of siliciclastic deposits on the north of the Imouzzer anticline and in the Amsittène anticline could be an accumulation induced by higher energy settings, linked to their location on topographic highs (Duval-Arnould, 2019). In the locations AMCA and ASH, the higher energy settings persist after the siliciclastic influx, and carbonates grainstones progressively replace the sandstones, before the onset of the generalized regression and the development of tidal-flat deposits all over the basin.

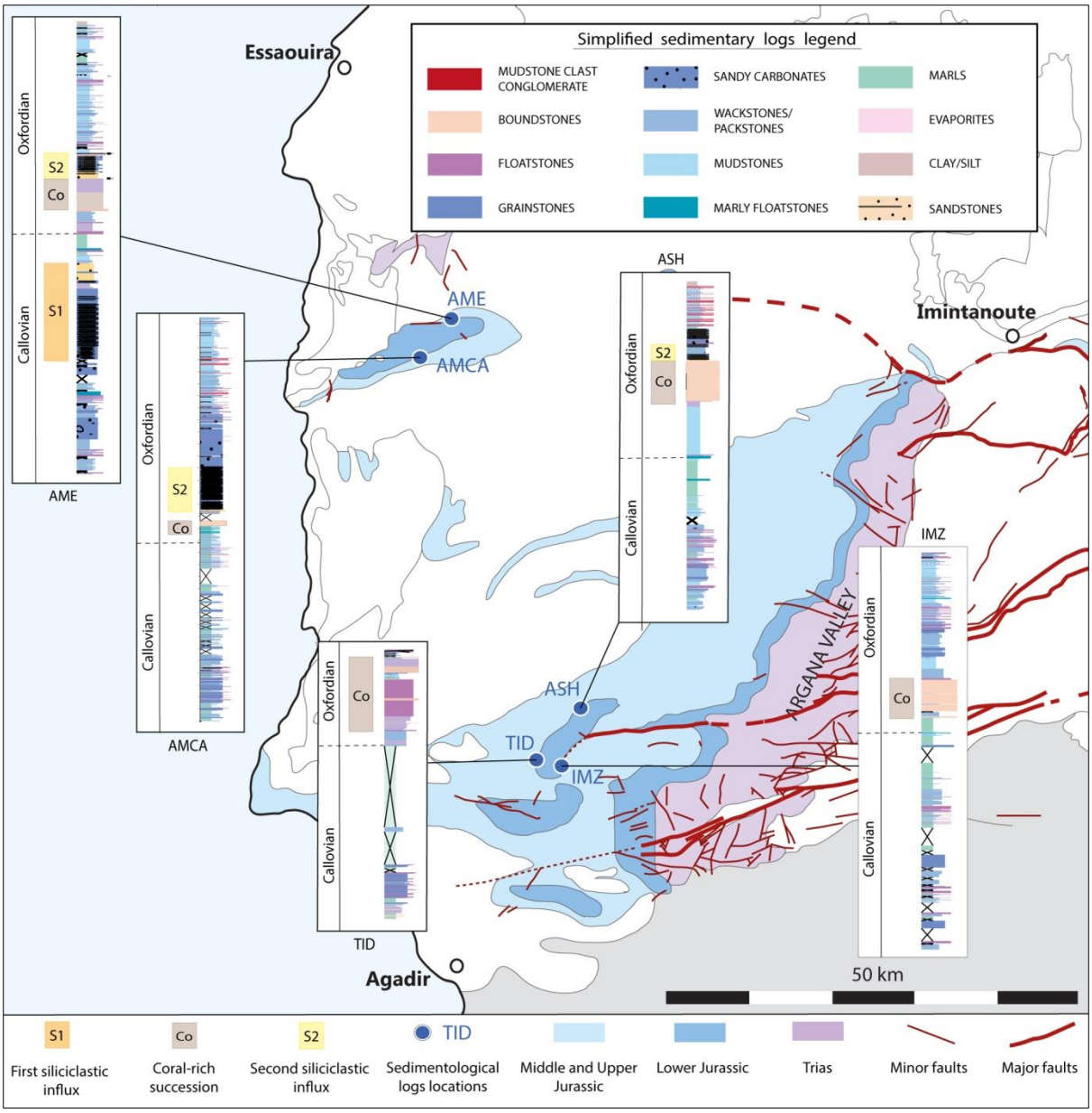

Figure C | Simplified logs from Jurassic outcrops in the studied anticlines (after Duval-Arnould, 2019)